RSC Advances

PAPER

View Article Online
View Journal | View Issue

Cite this: *RSC Adv.*, 2015, **5**, 4993

Green synthesis of zinc oxide nanoparticles using *Hibiscus subdariffa* leaf extract: effect of temperature on synthesis, anti-bacterial activity and anti-diabetic activity

Niranjan Bala,[a] S. Saha,[a] M. Chakraborty,[a] M. Maiti,[a] S. Das,*[a] R. Basu[b] and P. Nandy[c]

Received 20th October 2014
Accepted 10th December 2014

DOI: 10.1039/c4ra12784f

www.rsc.org/advances

Zinc oxide (ZnO) nanoparticles (NPs) have been synthesized using *Hibiscus subdariffa* leaf extract. Temperature dependent synthesis and particle growth have been studied. Formation of NPs was confirmed by UV-visible (UV-VIS) spectroscopy, Fourier transform infrared (FTIR) spectroscopy and X-ray diffraction (XRD). Electron microscopy has been used to study the morphology and size distribution of the synthesized particles. The synthesized ZnO nanoparticles as potential anti-bacterial agents have been studied on *Escherichia coli* and *Staphylococcus aureus*. Another study has indicated that small sized ZnO NPs, stabilized by plant metabolites had better anti-diabetic effect on streptozotocin (STZ) induced diabetic mice than that of large sized ZnO particles. It has also been observed by enzyme linked immunosorbent assay (ELISA) and real time polymerase chain reaction (RT-PCR) that ZnO can induce the function of Th1, Th2 cells and expressions of insulin receptors and other genes of the pancreas associated with diabetes.

1. Introduction

In recent years ZnO NPs have drawn attention of many researchers for their unique optical and chemical behaviors which can be easily tuned by changing the morphology. Within the large family of metal oxide NPs ZnO NPs have been used in various cutting edge applications like electronics, communication, sensors, cosmetics, environmental protection, biology and the medicinal industry.[1–5] Moreover, ZnO NP has a tremendous potential in biological applications like biological sensing, biological labeling, gene delivery, drug delivery and nanomedicine[5–8] along with its antibacterial, antifungal, acaricidal, pediculocidal, larvicidal and anti-diabetic activities.[9–13]

Recently, synthesis of NPs *via* eco-friendly routes have become popular among researchers due to its low cost, synthesis in ambient atmosphere, non-toxicity, environmental compatibility *etc.* and ease of applications as the resulting particles are highly soluble in water, biocompatible, and devoid of toxic stabilizers. Plant extracts are very promising tool for facile synthesis of NPs *via* green routes. *Citrus aurantifolia* fruit juice, *Parthenium hysterophorus* leaf extracts, *Aloe* sp. extracts have been used in ZnO NP synthesis by different workers.[14–16] *In vivo* synthesis of ZnO NP has been also reported in *Physalis alkekengi*.[17]

Hibiscus subdariffa L. (*H. sabdariffa* var. *sabdariffa* race: *albus*) belongs to Malvaceae family and commonly known as Indian sorrel. It is commonly cultivated for fiber and edible purposes and used as native medicine in India, Africa and Mexico. Leaf and calyx extract of the plant found to be diuretic, cholerectic, hypotensive, blood pressure suppressive, chemo-protective, antioxidant, anti-tumor and anti-cancerous agent.[18–22] It has been also reported that, *H. sabdariffa* is a very effective antimicrobial agent and helpful in diabetes mellitus.[23–26]

During our work, we have synthesized ZnO NP *via* green routes using *H. subdariffa* leaf extract, giving a special emphasize on growth of NP at different temperatures. Optical properties of the synthesized NPs were measured using UV-visible (UV-VIS) spectroscopy. Characterization of NPs had been done by X-ray diffraction (XRD) and Fourier transformed infrared spectroscopy (FTIR). Morphology of prepared samples was analyzed by field emission scanning electron microscopy (FESEM) and high resolution transmission electron microscopy (HRTEM) was used to investigate the particle size. Anti-bacterial assay has been performed. Anti-diabetic activity was also investigated suggesting probable mechanisms for their potential medicinal uses. Induction of cytokines and other regulatory genes associated with diabetes had been studied in response to ZnO treatments in animal model utilizing ELISA and RT-PCR techniques.

[a]*Department of Physics, Jadavpur University, Kolkata 700032, India. E-mail: sdasphysics@gmail.com*
[b]*Department of Physics, Jogamaya Devi College, Kolkata 700 026, India*
[c]*Centre for Interdisciplinary Research and Education, Kolkata 700 068, India*

2. Materials

Hibiscus subdariffa (Malvaceae) was collected from Jadavpur University campus. Streptozotocin (STZ), Zinc acetate dihydrate, tri-sodium citrate and other chemicals used in this experiment were purchased from Merck (India) and all are of research grade. *Escherichia coli* DH5α (MTCC 1652) and *Staphylococcus aureus* (MTCC 96) bacteria were purchased from IMTECH, Chandigarh, India. Male Swiss albino mice (20–25 days old) weighing 32 ± 5 g were obtained from animal house, approved by committee for the purpose of control and supervision of experiments on animal (CPCSEA), Chennai, India (Registration no. 50/CPCSEA/1999). The animals were divided into 4 groups and maintained under standard laboratory conditions (temperature 25 °C ± 2 °C with day/night circle of 12 h/12 h). Free access of dry plate diet (Hindustan Lever, Kolkata) and water *adlimitom* were provided. The experiments were carried out according to the guideline of CPCSEA and approved by the institutional animal ethics committee (approval no. TOX/DEY'S/IAEC/08/13).

3. Methods

3.1. Plant extracts preparation

5 grams of *H. sabdariffa* leaves were washed thoroughly with plenty of distilled water and both surface of leaves were sterilized using alcohol by gently rubbing. These leaves were heated for 30 min in 100 ml of distilled water at 50 °C. Then the extract was filtrated with Whatman filter paper no. 1 and further filtered using vacuum filter with pore size of 0.2 μm. The final filtrate was stored in cool dry place for further use.

3.2. Green synthesis of zinc oxide nanoparticles

20 ml of the plant extract was heated at 50 °C for 10 min and 50 ml of 91 mM of zinc acetate solution (1 g of zinc acetate was dissolved in 50 ml of distilled water) was added drop wise to it under stirring. The reaction mixture became yellowish and cream coloured precipitate of zinc hydroxide was formed. The reaction mixture was left for 30 min for complete reduction to zinc hydroxide. Then the precipitate was collected by centrifugation at 16 000 rpm for 10 min at 4 °C. The precipitate was vacuum dried at 30 °C and the sample (PZN30) was stored for further studies. Two other samples were prepared by heating PZN30 for 4 hours at 60 °C (PZN60) and 100 °C (PZN100).

Effect of plant extract on synthesis of ZnO NP was investigated by varying the ratio of plant extract to zinc acetate (v/w) and was represented by yield of ZnO, calculated by using following formula

$$\text{Yield (\%)} = (\text{experimental weight of ZnO/theoretical weight of ZnO}) \times 100.$$

3.3. Phytochemical analysis of the plant extract

3.3.1. Total phenolic content. Total phenolic content of the plant extract was determined by following the procedure of Luximon-Ramma *et al.*[27] Phenolic content was expressed in terms of μg of gallic acid equivalent per ml of plant extract.

3.3.2. Total flavonoid content. Flavonoid contents in plant extract were measured following the protocol of Ghosh *et al.*[28] and were expressed in μg of quercetin equivalent per ml of plant extract.

3.3.3. Reducing sugar content. Reducing sugar content present in plant extract was estimated following the procedure of Bala *et al.*[29] and was expressed in μg of maltose equivalent per ml of plant extract.

3.3.4. Starch content. Total starch content in plant extract was measured following the protocol of Thayumanavan *et al.*[30] and was expressed in μg of glucose equivalent per ml of plant extract.

3.4. Characterization of NPs

UV-VIS light spectra of the synthesized nanoparticles were recorded (λ25 spectrophotometer, Perkin Elmer Germany). Same amount of different samples were considered for UV-VIS data analysis.

XRD patterns of the synthesized materials were analyzed in the range of 2θ from 20° to 80° using powder diffractometer, Model D8, BRUKER AXS, by Cu K_α radiation ($\alpha = 0.15425$ nm).

FTIR was recorded in JASCO FTIR instrument-410 (USA). 1% KBr plate of the powder samples and lyophilized plant extract were prepared for analyzing chemical constituents present in samples.

Surface morphology and elemental analysis of the samples were analyzed by FESEM coupled with Energy dispersive X-ray spectroscopy (EDX) using INSPECT F50 (FEI, Netherland). For FESEM study, dry powder samples were sprayed over the carbon tape and coated with gold. Shape and particle size distribution of PZN60 and PZN100 solutions were analyzed by HRTEM using JEM – 2100 HRTEM (JEOL, Japan).

3.5. Anti-bacterial assay

Anti-bacterial activities were studied against *Escherichia coli* DH5α (MTCC 1652) and *Staphylococcus aureus* (MTCC 96) strain. Interaction between NPs and bacteria were studied following the standard protocol, where 0–500 μg ml^{-1} of synthesized powder samples were added to cultures of bacteria (10^7 CFU ml^{-1}) in 5 ml nutrient broth (0.5% peptone, 0.1% beef extract, 0.2% yeast extract, 0.5% NaCl, pH 7). The cultures were then incubated at 37 °C for 24 h. Inhibition of bacterial growth was observed by plating 20 μl of the treated culture on nutrient agar (nutrient broth with 1.5% agar as the solidifying agent) plates for 24 h. Colony forming units of bacteria were counted and compared with control after 24 h incubation at 37 °C. The whole experiment was repeated thrice. Minimum inhibitory concentration (MIC) and minimum bactericidal concentration (MBC) of samples were determined using agar broth dilution method and standard plate count technique respectively.

Time dependent growth of bacteria was also studied. The vulnerability of the tested bacteria was checked in various time intervals by observing optical density at 600 nm.

3.6. Experimental design for anti-diabetic test

Anti-diabetic studies were done with the mice divided into 4 groups ($n = 5$). Diabetes induced in mice by STZ and cured by intraperitoneal injection of ZnO once in every alternate day. Table 1 summarizes the treatment for each group.

3.7. Induction of diabetes

Diabetes was introduced in experimented mice by a single intraperitoneal dose of 100 mg kg^{-1} STZ in 10 mM sodium citrate buffer (pH 4.5). After STZ treatment, mice were fed with high sucrose and high fat diet. Fasting blood glucose was measured regularly and the mice with blood glucose above 250 mg dl^{-1} were treated as diabetic. Blood glucose level was measured every day from tail vain using AccuCheck, blood glucose monitor kit (Germany) of each group. Total duration of the experiments was 28 days, at the end of which the animals were fasted overnight, anesthetized with anesthetic ether and killed by survical dislocation. Different tissues were dissected out and wiped clear to remove adhering blood and stored in vacuum desiccators at −20 °C to prevent exposure to auto-oxidation environment and were used for future study.

3.8. ELISA test

Cytokine profiles of mice were determined using commercial ELISA kits (R & D System, Minneapolis, MN, USA). The levels of tumor necrosis factor-α (TNF-α), interleukin (IL)-1β, interleukin (IL)-6, interleukin (IL)-4 and interleukin (IL)-10 in pancreas tissue were studied. The assays were performed following the instructions supplied by the respective Quantikine Immunoassay Kit (Minneapolis, U.S.A.).

3.9. Molecular biological parameters estimation of mice by RT-PCR

Molecular biological parameters were estimated following the protocol of Alkaladi *et al.* (2014). Total RNA from the pancreas tissue were extracted using MagJET RNA Kit (Thermo scientific, USA) and RevertAid H Minus First Strand cDNA Synthesis Kit (Thermo scientific, USA) was used for cDNA synthesis. Every RT reaction contained 1 μg RNA template, 1 μl random hexamer primer, 4 μl 5× reaction buffer (250 mM Tris–HCl (pH 8.3), 250 mM KCl, 20 mM $MgCl_2$, 50 mM DTT), 1 μl, 20 U μl^{-1} RibolockRNase inhibitor (Thermo scientific, USA), 2 μl, 10 mM dNTP Mix (Thermo scientific, USA) and 1 μl, 200 U μl^{-1} RevertAid H Minus M-MuLV Reverse Transcriptase (Thermo scientific, USA). The PCR reaction was started by 2× Dream Taq Green PCR Master Mix (Thermo scientific, USA). The reaction was performed using Light Cycler® 480 Real-Time PCR (Roche Applied Science, Penzberg, Germany). Agarose gel electrophoresis of amplified PCR products of selected genes were visualized using UV-trans illuminator. GAPDH was used as reference control. Primers (Operon Biotechnologies, Gmbh, Germany) for selected genes were as follows,

Insulin receptor A (*IR A*)	Forward, 5′-TTC ATT CAG GAA GAC CTT CGA-3′ Reverse, 5′-AGG CCA GAG ATG ACA AGT GAC-3′
Glucose transporter-2 (*GLUT 2*)	Forward, 5′-TTA GCA ACT GGG TCT GCA AT-3′ Reverse, 5′-TCT CTG AAG ACG CCA GGA AT-3′
Glucokinase (*Gk*)	Forward, 5′-CAC CCA ACT GCG AAA TCA CC-3′ Reverse, 5′-CAT TTG TGG GGT GTG GAG TC-3′
Pyruvate kinase (*PKLR*)	Forward, 5′-CTGGAACACCTCTGCCTTCTG-3′ Reverse, 5′-CACAATTTCCACCTCCGACTC-3′
TNF-α	Forward, 5′-GGCAGGTCTACTTTGGAGTCATTGC-3′ Reverse, 5′-ACATTCGAGGCTCCAGTGAATTCGG-3′
IL-1β	Forward, 5′-TTGACGGACCCCAAAAGAT-3' Reverse, 5′-GAAGCTGGATGCTCTCATCTG-3′
IL-6	Forward, 5′-TGGAGTCACAGAAGGAGTGGCTAAG-3′ Reverse, 5′-TCTGACCACAGTGAGGAATGTCCAC-3′
IL-4	forward, 5′-ATG GGT CTC AAC CCC CAG CTA GT-3′ Reverse, 5′-GCT CTT TAG GCT TTC CAG GAA GTC-3′
IL-10	Forward, 5′-CGGGAAGACAATAACTG-3′ Reverse, 5′-CATTTCCGATAAGGCTTGG-3′
GAPDH	Forward, 5′-CCC GTA GAC AAA ATG GTG AAG GTC-3′ Reverse, 5′-GCC AAA GTT GTC ATG GAT GAC C-3′

4. Result and discussion

4.1. Dependence of plant extract concentration on ZnO NP synthesis

Concentration of plant extract plays a vital role in the synthesis of ZnO NPs. It has been observed that the ratio of plant extract to zinc acetate 20 ml g^{-1} (*i.e.* 1 g of zinc acetate in 20 ml of plant extract) was optimal concentration for the synthesis of ZnO NPs. Insufficient amount of bioactive compound present in 5–15 ml g^{-1} of zinc acetate lowers the yield of ZnO, whereas, 20–25 ml g^{-1} of zinc

Table 1 Treatments of mice for each group in anti-diabetic studies

Set	Drug for diabetic induction	Drug for treatment
Group I	Control	Control
Group II	STZ (100 mg kg^{-1} body weight)	None
Group III	STZ (100 mg kg^{-1} body weight)	PZN60 (8 mg kg^{-1} body weight)
Group IV	STZ (100 mg kg^{-1} body weight)	PZN100 (8 mg kg^{-1} body weight)

acetate yield nearly same amounts of ZnO (Fig. 1A). That means, amount of bioactive compounds present in case of 20 ml g^{-1} was sufficient to reduce all Zn^{2+} ions present in the reaction mixture.

4.2. Effect of temperature on ZnO NP synthesis

Dried precipitate was optically analyzed by UV-VIS spectroscopy. From the UV-VIS spectra (Fig. 1B) it was clear that, sample dried at 30 °C (PZN30) showed no characteristics absorption band, indicating the absence of ZnO NPs, while ZnO dried at 60 °C (PZN60) and 100 °C (PZN100) showed sharp surface plasmon resonance (SPR) bands at 377 nm confirming the presence of ZnO NPs. Samples calcinated at 100 °C showed higher absorption intensity than that calcinated at 60 °C, which was due to formation of more intense phases of ZnO NPs.

XRD patterns of the samples were shown in Fig. 2A–C. XRD shows 2θ values at 31.77°, 34.40°, 36.22°, 47.61°, 56.58°, 62.85°, 66.41°, 67.93°, 69.08°, 72.54° and 76.85° corresponds to (100), (002), (101), (102), (110), (103), (200), (112), (201), (004) and (202) planes confirmed the presence of ZnO NPs. All the peaks were duly assigned using JCPDS file no. 361451. The characteristics peaks for ZnO were present in the XRD patterns of sample PZN60 and PZN100. However, sample PZN30 was devoid of such characteristic peaks as it was amorphous in nature. XRD spectra confirmed that ZnO formation started above 30 °C and crystallinity of the sample increased with increase in temperature.

4.3. Functional groups being involved in ZnO NPs synthesis

FTIR spectra showed presence of characteristic bands for several functional groups in aqueous extract of *H. subdariffa*, PZN60 and PZN100 (Fig. 2D, E and F) respectively. IR peaks for –OH stretching of water was observed at around 3441, 3478 and 3450 cm^{-1}.[31] Aromatic compounds were present and confirmed by C=C stretching of aromatic amine, aromatic C–H, asymmetric stretch of C=C–C, symmetric stretch of –C–C=C and C=C were observed at around 1381, 2889, 1474, 1576 and 1780 cm^{-1},[31,32] Bending vibration of the alcoholic –C–OH, $-NH_2$ stretching vibration of secondary amine and –C=O groups from the aromatic ring having conjugation were reflected from the presence of peak at 1102, 1629 and 1422 cm^{-1}.[33] Presence of ZnO was confirmed by a peak at 482 cm^{-1} in both PZN60 and PZN100.[34] Peaks for glycosidic linkage of C–O–C and secondary alcoholic group were observed at 1565 and 1225 cm^{-1} respectively.[35,36] Current findings are supported by some previous reports on phytochemical constituents of *H. subdariffa*.[37] Aqueous extract of plant contains phenolic compounds, flavonoids, saponins, tannins and alkaloids, amines.[37] IR bands of these compounds justified their presence.

A significant difference in the FTIR spectra of PZN60 and PZN100 were observed. FTIR spectrum of PZN60 confirmed the presence of intense stretching and vibrational bands for several compounds. FTIR spectrum for PZN60 showed characteristic vibrational bands of aromatic compounds around 1381, 2889, 1474, 1576 and 1780 cm^{-1} which correspond to C=C stretching of aromatic amine, aromatic C–H, asymmetric stretching of C=C–C, symmetric stretch of –C–C=C and C=C respectively.[31,32] Bending vibration of the alcoholic –C–OH, –C=O groups from the aromatic ring having conjugation and secondary alcoholic group were reflected at 1102, 1422 cm^{-1} and 1225 cm^{-1}.[33,36] This result supported that, bioactive compounds were absorbed on the surface of ZnO particles in PZN60. On the other hand FTIR spectrum of PZN100 showed that those phytoactive compounds were either absent or remained absorbed on ZnO nanoparticles in small amount. These differences were due to rise in temperature as the bioactive compounds were lost in PZN100 as they were calcinated at higher temperature.

4.4. Phytochemical analysis

Phytochemical analysis of plant extracts supported the results obtained from FTIR. It was observed that phenolics, flavonoids, ascorbic acid, reducing sugar and starch present in the plant extract (Table 2) can trigger reduction of zinc acetate and control the size of synthesized nanoparticles.

The underlying mechanism for green synthesis of ZnO NPs has not been fully understood as yet. Free amino and carboxylic groups of proteins, alkaloids, phenolics or flavonoids, present in the plant extract may bind to the surface of zinc (Zn^{2+}) and trigger the formation of ZnO NPs. Amide from proteins and

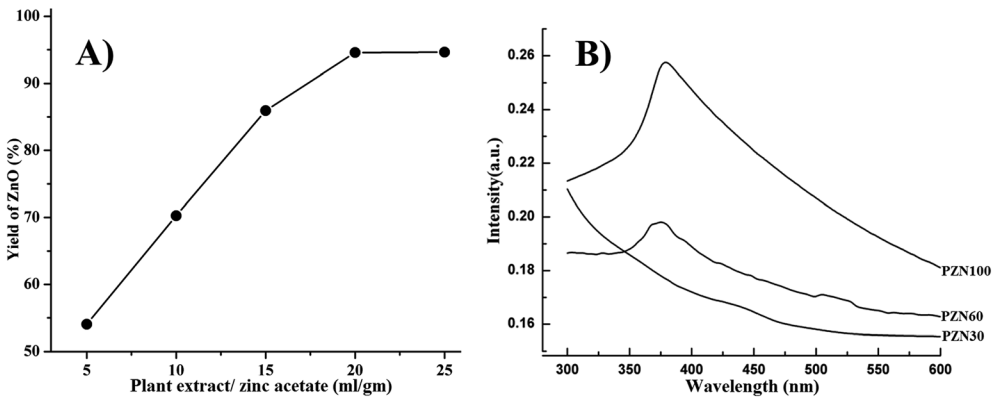

Fig. 1 (A) Effect of plant extract/zinc acetate ratio on yield (%) of ZnO NPs synthesis using this green route; (B) UV-VIS spectra of PZN30, PZN60 and PZN100.

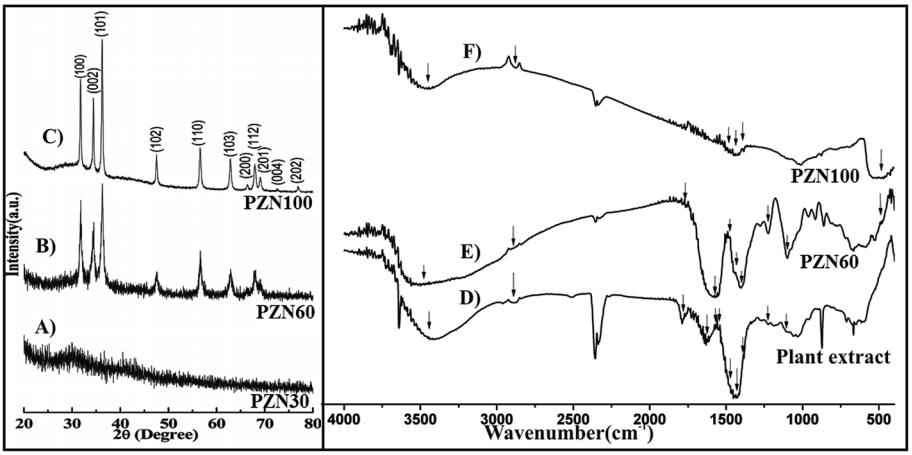

Fig. 2 (A), (B) and (C) XRD of PZN30, PZN60 and PZN100 respectively showing appearance of peaks for ZnO at higher temperature; (D), (E) and (F) FTIR spectra of lyophilized plant extract, PZN60 and PZN100 respectively showing appearance of transmittance bands (with arrow) for different functional groups of plant extract associated with ZnO NPs.

Table 2 Phytochemical analysis of plant extracts. Values represented in table were mean ± SD

Phytochemicals	Amount (μg ml^{-1})
Total phenolics	9.35 ± 0.32
Flavonoids	4.75 ± 0.29
Reducing sugar	458 ± 12.3
Starch	447 ± 9.5

C═O, C═O–C and C═C groups of heterocyclic compounds may act like a stabilizer.[31–33]

4.5. Effects of temperature on surface morphology of ZnO NPs

Surface morphology of NPs were thoroughly studied by FESEM micrographs. From the micrographs (Fig. 3), it was observed that PZN30 showed irregular surface morphology (Fig. 3A and B) and was amorphous in nature, previously confirmed by XRD (Fig. 2). Spherical structure was found in PZN60 (Fig. 3C and D), which on higher magnification showed aggregation of group of smaller spherical particle ranging from 16–60 nm (showed in arrow) together forming cauliflower like structure around 300–400 nm in diameter. PZN100 was more crystalline in nature and were forming a dumbbell shaped structure (showed in arrow) with a length of 200–230 nm, 30–50 nm diameter in head and 70–80 nm broad at base region (Fig. 3E and F). The transformation of shape in PZN100 was induced by crystal growth and loss of bioactive compounds (stabilizers) of PZN60 due to higher temperature. The smaller particles in PZN60 became aligned and the crystals grew in such a way that outer particles formed the head and central parts of the aggregates formed the body of dumbbell structure in PZN100.

HRTEM micrograph (Fig. 4) analysis confirmed the shape and size of synthesized ZnO NPs obtained from FESEM. FESEM micrographs of PZN60 showed agglomerated particles indicating larger size and low surface to volume ratio than PZN100. But, isolated small sized particles with 12–46 nm in diameter (Fig. 4A) were observed by HRTEM in aqueous solution of PZN60. It clearly demonstrated that, aggregated mass of

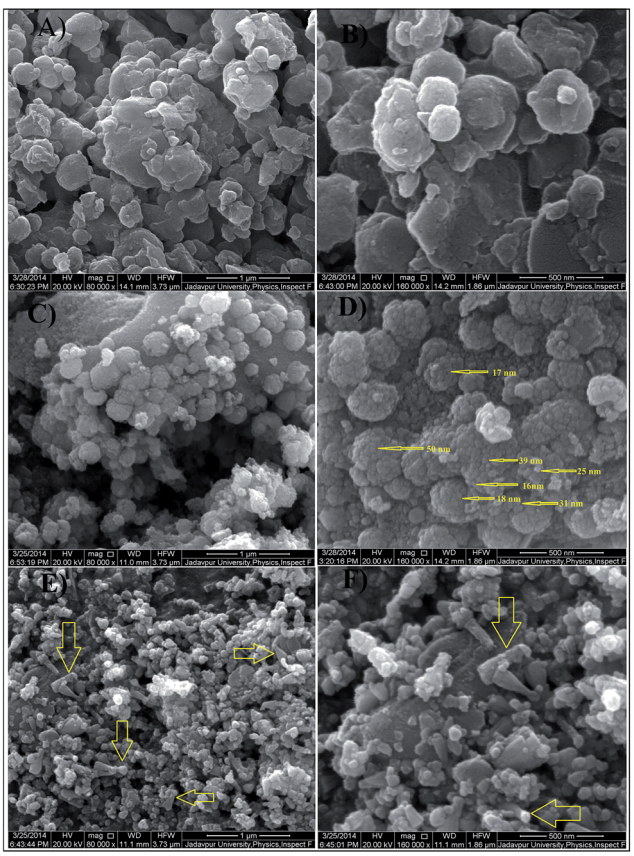

Fig. 3 FESEM micrograph of synthesized ZnO. (A) PZN30 at 1 μm scale; (B) PZN30 at 500 nm scale; for PZN60 particles were spherical in nature and each particle was aggregation of many smaller particles. (C) PZN60 at 1 μm scale; (D) PZN60 at 500 nm scale. For PZN100 dumbbell shaped larger particles due to crystal growth. (E) PZN100 at 1 μm scale; (F) PZN100 at 500 nm scale.

particles were lost its arrangement patterns in solution phase resulting smaller size and higher surface to volume ratio than that of 190–250 nm dumbbell shaped particles (Fig. 4B) observed in PZN60.

EDX of the samples (Fig. 5) indicated the presence of zinc and oxygen at stoichiometric ratio. Carbon, nitrogen and some other element in the EDX spectra showed the presence of stabilizing agents which were originated from plant extract. Presence of carbon and nitrogen in Fig. 5B indicating bioactive compounds were adsorbed on PZN60 which were absent in PZN100 (Fig. 5C) due to temperature rise.

4.6. Anti-microbial activity of ZnO NPs

Anti-microbial effects of ZnO NPs synthesized *via* green routes were investigated. ZnO NPs exert their bactericidal property on *E. coli* and *S. aureus*. It was observed that the anti-bacterial activity of sample PZN60 was better than that of samples PZN30 and PZN100 (Fig. 6). In Fig. 6, *E. coli* and *S. aureus* were treated with 300 μg of PZN30 (Fig. 6A and D), PZN60 (Fig. 6B and E) and PZN100 (Fig. 6C and F) but, better result were observed for PZN60. Sample PZN30 was basically $Zn(OH)_2$ which showed less anti-bacterial activity than ZnO NPs. But the difference in activities of PZN60 and PZN100 was due to variation in particle size and presence of phytochemicals originated from plant extracts. Smaller particles of PZN60 possess higher surface to volume ratio and more bioactive compounds of the plant extract than that of PZN100. PZN60 due to its smaller size penetrate easily within the bacterial cell and exert better bactericidal effect.

Results from anti-bacterial assay supported that *E. coli* was more susceptible to ZnO NPs than *S. aureus* which is supported by the works of Applerot *et al.*[9] Anti-bacterial activity of *H. subdariffa* was previously investigated by several researchers.[23,24] It was evident that standard gram positive bacterial strains were more susceptible to *H. subdariffa* extract than gram negative strains. NPs synthesized *via* this route showed better result on both gram positive and gram negative strains, as they were stabilized by different secondary metabolites of *H. subdariffa*.

MIC and MBC values for *E. coli* was slightly lower (Fig. 7) than that of *S. aureus*. It was evident from Fig. 8 that, green ZnO NPs showed well bactericidal efficiency at concentration higher than that of 50 μg ml^{-1}. MBC of *E. coli* and *S. aureus* were found to be better in sample treated with PZN60 than that treated with PZN100.

The mechanism of anti-bacterial effect of ZnO NPs synthesized *via* green route may be explained as follows: Gram negative strains are sensitive to pure ZnO NPs[24] whereas ZnO inhibits the growth of gram negative strains mainly by ROS

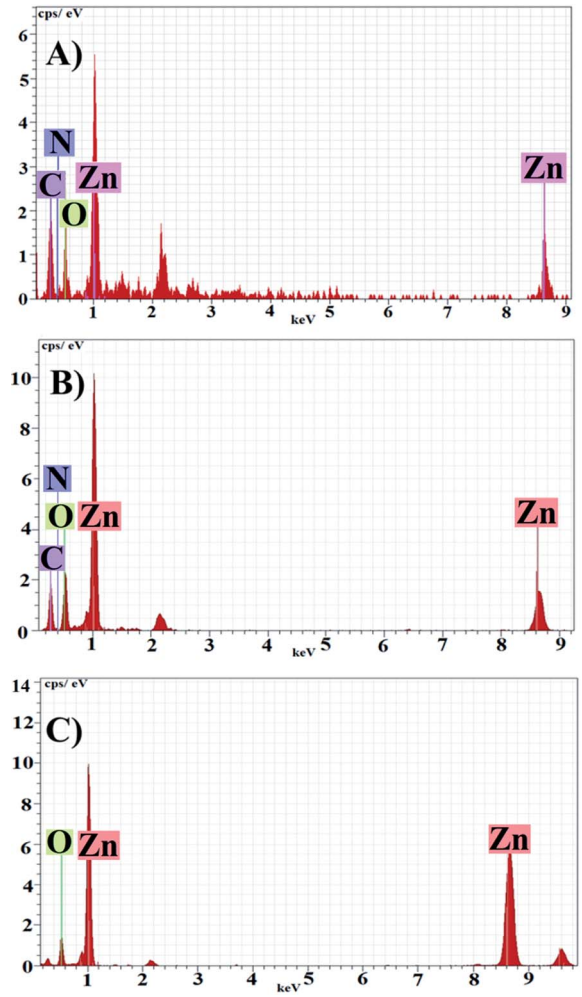

Fig. 5 EDX spectra of sample (A) PZN30, (B) PZN60 and (C) PZN100.

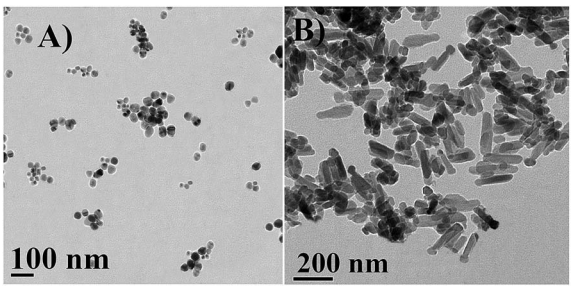

Fig. 4 HRTEM micrograph of synthesized ZnO. (A) Isolated spherical particles of PZN60, size ranging from 12–46 nm at 100 nm scale bar; (B) dumbbell shaped particles of PZN100, size ranging from 190–250 nm in lengths and 50–60 nm in breadths at 200 nm scale bar.

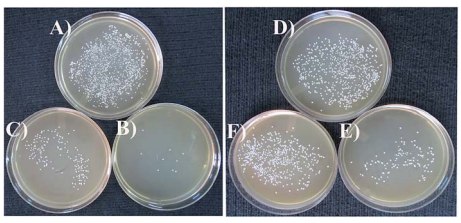

Fig. 6 Anti-microbial effects of green ZnO NPs; *E. coli* treated with (A) 300 μg ml^{-1} of PZN30, (B) 300 μg ml^{-1} of PZN60 and (C) 300 μg ml^{-1} of PZN100 cultured on agar plates. *S. aureus* treated with (D) 300 μg ml^{-1} of PZN30, (E) 300 μg ml^{-1} of PZN60 and (F) 300 μg ml^{-1} of PZN100 cultured on agar plates.

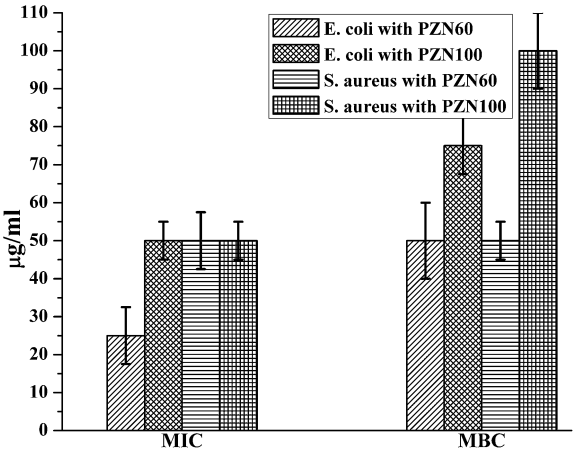

Fig. 7 MIC and MBC values of *E. coli* and *S. aureus* treated with PZN60 and PZN100.

generation,[11] size and surface area of the particles were also key factors.[38,39]

On the contrary, gram positive strains are susceptible to phytochemicals of *H. subdariffa* like polyphenols, flavonoids *etc.* which were adsorbed on surface of ZnO NPs. Flavonoid forms complex structures with cell wall materials and increases plasma membranes permeability, finally ion leaching.[40,41] Hydroxylation of cell wall is also triggered by the hydroxyl group of polyphenols which becomes toxic to bacterial cell.[40]

From the above observations it can be concluded that, PZN60 was more efficient bactericidal agent than that of PZN100. Enhancement of anti-bacterial efficacy was triggered by smaller size and sufficient amount of bioactive compounds adsorbed on PZN60. Calcination at 100 °C results larger size due to crystal growth and loss of major phytochemicals from the surface of PZN100 lowers its anti-bacterial efficiency on both the bacterial strains.

FESEM micrographs (Fig. 9 and 10) of bacterial samples before and after PZN60 treatments were investigated suggesting probable reasons responsible for its antibacterial activity. Bacteria without PZN60 treatment shows normal rod like (Fig. 9A) and spherical (Fig. 10A) morphology with uninterrupted cell wall of *E. coli* and *S. aureus* respectively. PZN60 treatment results cell damaged due to ruptured cell wall and pore formation (Fig. 9B and 10B). These triggers leakage of ions and cellular materials ultimately cell death.

4.7. Anti-diabetic activity of ZnO NPs

Anti-diabetic activity of synthesized green ZnO NPs were investigated on mice for their potential therapeutic effects against STZ induced hyperglycemia. In this current study we have investigated anti-diabetic activity of green ZnO NPs sintered at two different temperatures *i.e.* 60 °C (PZN60) and 100 °C (PZN100). It was observed there was a significant enhancement of blood glucose level in mice treated with STZ and which was restored after ZnO NP treatments (Fig. 11A). Reduction of blood glucose level in mice treated with PZN60 and PZN100 were 59.58% and 48.27% respectively than that of untreated.

STZ induced diabetes was associated with chronic inflammation due to the expression of pro-inflammatory cytokines like TNF-α, IL-6, IL-1β which induces pancreatic β cell apoptosis,[42] cardio-vascular injury such as neuropathy, retinopathy and nephropathy[43] due to endothelial dysfunction.[44]

ELISA result of cytokines demonstrated the imbalance between Th1 and Th2 cell, in which Th1 representing cytokines (TNF-α, IL-1β, IL-6) were increased rapidly after diabetic induction (Fig. 11B), whereas, the increment levels of Th2 representing cytokines (IL-4, IL-10) were decreasing in this condition. Those effects were also diminished by PZN60 supplementation to the animals. After diabetic induction, the secretion level of TFN-α, IL-1β and IL-6 were 3.16 fold, 2.7 fold

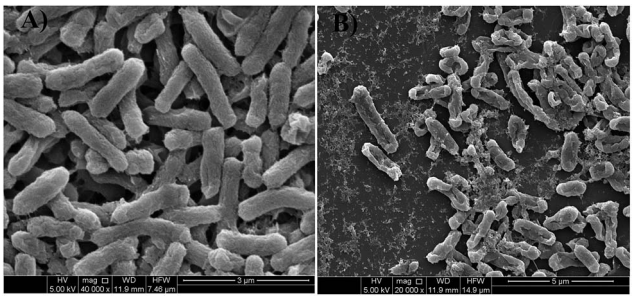

Fig. 9 FESEM micrographs of (A) *E. coli* without PZN60 treatment and (B) *E. coli* treated with 300 µg ml^{-1} of PZN60.

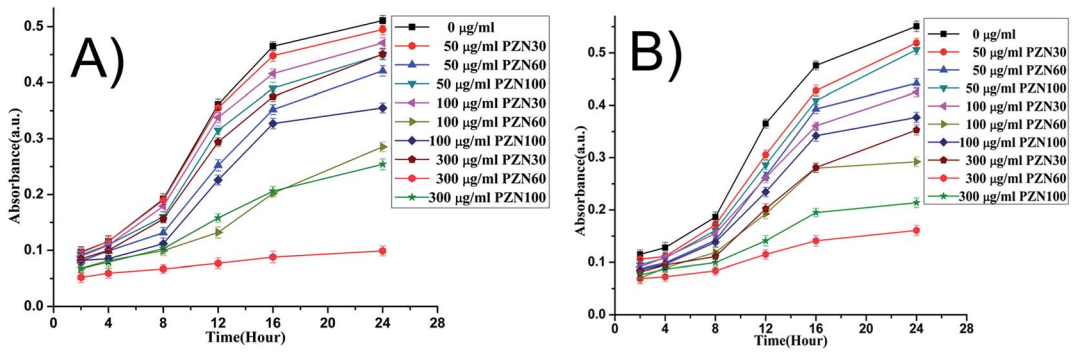

Fig. 8 Time dependent growth pattern of *E. coli* and *S. aureus* treated with 0, 50, 100 and 300 µg ml^{-1} of synthesized NP.

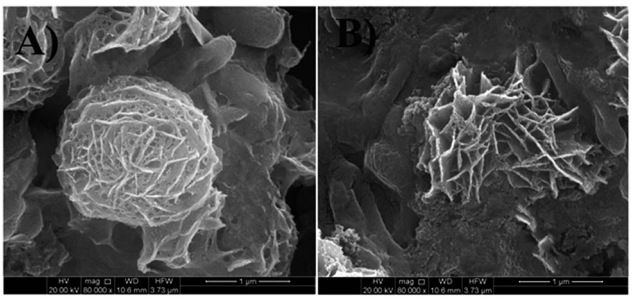

Fig. 10 FESEM micrographs of (A) *S. aureus* without PZN60 treatment and (B) *S. aureus* treated with 300 μg ml^{-1} of PZN60, arrows showed the presence of ZnO on damaged bacteria.

and 2.75 respectively more than control groups. The increment level of IL-4 was 2.1 fold and IL-10 was 2.45 fold lower than corresponding control groups. The ameliorative activity of PZN60 was more in each case than that of PZN100.

The mRNA expressions were monitored by RT-PCR to study the effects of STZ, PZN60 and PZN100 treatments on the inflammatory cytokine and other receptor genes associated with diabetes (Fig. 12). Constant over expression of TFN-α, IL-1β and IL-6 were observed in pancreatic cells of diabetes induced mice in comparison to their respective controls (Fig. 12A). Administration of PZN60, PZN100 resulted in down regulation of these molecules with respect to their diabetic-induced expression. But the expression levels of IL-4 and IL-10 decreased significantly than their corresponding control group, which was normalized after PZN60 treatment. The difference in expressions of TFN-α, IL-1β and IL-6 indicated that the basal level of TFN-α and IL-6 was higher in body than that of IL-1β. Diabetes induced condition down regulated the expression of IL-4 and IL-10 cytokines. PZN60 treatment suppressed TFN-α, IL-1β and IL-6 expression and enhanced IL-4 and IL-10 expression more effectively against diabetic induction. The mRNA expression level of receptor genes like *IR A*, *GLUT 2* and *GK* were down-regulated and expression of *PKLR* was up-regulated due to diabetic induction, which was further down regulated by PZN60, PZN100 (Fig. 12B). The basal level of *GK* concentration was lower in comparison to *IR A*, *GLUT 2*. *GK* was involved in the first step of glucose utilization in pancreas which enhanced glucose uptake in liver and insulin secretion in pancreas.[45] Expression of *GLUT 2* was studied in relation with pathogenesis of diabetes. Down regulation of *GLUT 2* resulted in defective glucose stimulated insulin release in diabetes.[46]

STZ enters in pancreatic β-cell *via GLUT 2* (ref. 47) and induces alkylation of DNA causing DNA damage[48,49] which was activates poly ADP ribosylation. Cellular NAD^+ and ATP dephosphorylation lead to formation of superoxide radicals. Toxic amounts of peroxide, hydroxyl, superoxide and nitric oxideradicals[48] result in β cell destruction.[50]

The exact reason behind ZnO NP induced secretion of insulin is yet to be understood. It was thought that Zn^{2+} ions released from ZnO NPs might induce enhancement of insulin secretion from pancreatic islets. Insulin is stored in pancreas in the form of hexamer together with two Zn^{2+} ions.[51] Previous reports suggested less degradation of insulin in insulin-liver membrane complex induced by Zn^{2+} ions.[52] Zinc plays very important role in insulin action and carbohydrate metabolism.[53] Zinc can improves fasting insulin level and fasting glucose was observed in *in vivo* studies.[54]

From the results it can be concluded that the effectiveness of PZN60 was more than PZN100 against STZ induced diabetes in mice. Possibly, there are two different reasons behind these results. Smaller particle size of PZN60 caused better penetration in mice and better activity due to higher surface to volume ratio. On the other hand larger particles of PZN100 showed less penetration and lower activity due to reduced surfaces to volume ratio than that of PZN60.

Nature of synthesized ZnO NPs was another reason. PZN60 gets stabilized by several polyphenols and flavonoids of *H subdariffa* which inhibit α-amylase and α-glycosidase.[55] It has potency of anti-diabetic activity by reducing oxidative stress associated with diabetes.[25,26,56,57] But PZN100 calcinated at 100 °C for 4 hour lost the associated bioactive stabilizer compounds. These bioactive compounds together with ZnO

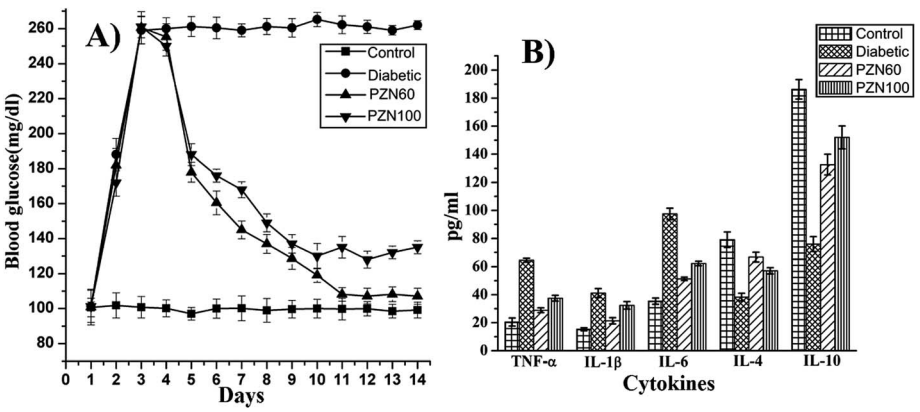

Fig. 11 (A) Blood glucose level in experimented mice, blood glucose levels increased after STZ treatment and was restored to near normal level after ZnO NP treatment; (B) level of inflammatory cytokines expression obtained from ELISA, expression level of TNF-α, IL-1β and IL-6 were over expressed while IL-4 and IL-10 were under expressed in diabetic mice. Their levels were restored to near control after ZnO treatments.

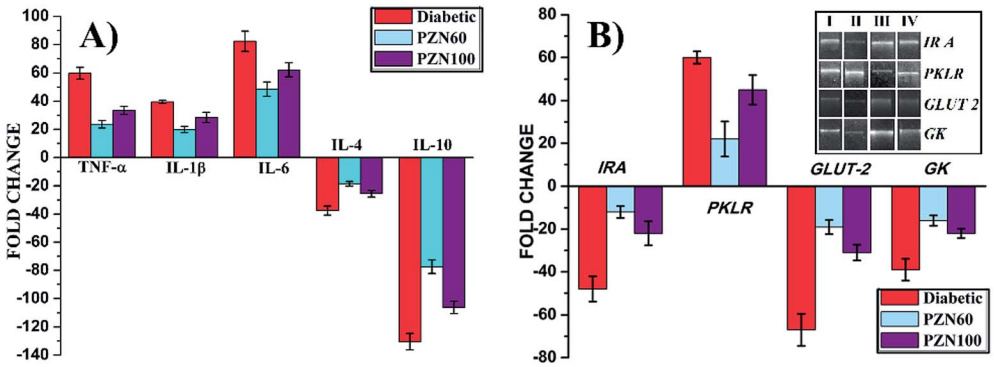

Fig. 12 m-RNA expression of different genes associated with diabetes. (A) m-RNA expressions of inflammatory cytokine genes in pancreas and (B) m-RNA expressions of different receptor genes associated with diabetes; DNA gel of different receptor genes after RT-PCR (inset).

NPs in PZN60 performed better anti-diabetic effect on STZ induced mice.

5. Conclusion

ZnO NP synthesized using the described route in this study has many advantages over other green routes. This process is both energy and cost effective with a high particle yield at lower concentration of plant extract. Particles are highly stable and showed high solubility in water. Size as well as efficacy may be tuned by temperature variation. It can be used in medicinal industries due to its potential ROS independent anti-bacterial effect and very effective anti-diabetic activity on Swiss albino mice at a very low concentration.

Acknowledgements

Defense Research and Development Organization is acknowledged for the financial support. M. Sarkar, Jadavpur University is also acknowledged for his support in manuscript preparation.

References

1 C. Dagdeviren, S. W. Hwang, Y. Su, S. Kim, *et al.* Transient, Biocompatible Electronics and Energy Harvesters Based on ZnO, *Small*, 2013, **9**(20), 3398–3404.
2 L. Wang, Y. Kang, X. Liu, S. Zhang, *et al.* ZnO nanorod gas sensor for ethanol detection, *Sens. Actuators, B*, 2012, **162**(1), 237–243.
3 S. E. Cross, B. Innes, M. S. Roberts, T. Tsuzuki, *et al.* Human skin penetration of sunscreen nanoparticles: *in vitro* assessment of a novel micronised zinc oxide formulation, *Skin Pharmacol. Physiol.*, 2007, **20**(3), 148–154.
4 J. Zhou, N. Xu and Z. L. Wang, Dissolving behavior and stability of ZnO wires in biofluids: a study on biodegradability and biocompatibility of ZnO nanostructures, *Adv. Mater.*, 2006, **18**(18), 2432–2435.
5 J. W. Rasmussen, E. Martinez, P. Louka and D. G. Wingett, Zinc oxide nanoparticles for selective destruction of tumor cells and potential for drug delivery applications, *Expert Opin. Drug Delivery*, 2010, **7**(9), 1063–1077.
6 S. H. Yoon and D. J. Kim, Fabrication and Characterization of ZnO Films for Biological Sensor Application of FPW Device. Applications of ferroelectrics, 15th IEEE international symposium on the July 30 2006–August 3 2006, 322–325.
7 H. M. Xiong, ZnO Nanoparticles Applied to Bioimaging and Drug Delivery, *Adv. Mater.*, 2013, **25**(37), 5329–5335.
8 L. Nie, L. Gao, P. Feng and J. Zhang, Three-Dimensional Functionalized Tetrapod like ZnO Nanostructures for Plasmid DNA Delivery, *Small*, 2006, **2**(5), 621–625.
9 G. Applerot, A. Lipovsky, R. Dror and N. Perkas, Enhanced antibacterial activity of nanocrystalline ZnO due to increased ROS-mediated cell injury, *Adv. Funct. Mater.*, 2009, **19**(6), 842–852.
10 D. Sharmaa, J. Rajputa, B. S. Kaitha and M. Kaurb, Synthesis of ZnO nanoparticles and study of their antibacterial and antifungal properties, *Thin Solid Films*, 2010, **519**(3), 1224–1229.
11 S. Nair, *et al.* Role of size scale of ZnO nanoparticles and microparticles on toxicity toward bacteria and osteoblast cancer cells, *J. Mater. Sci.: Mater. Med.*, 2009, **20**(Suppl. 1), S235–S241.
12 A. V. Kirthi, A. A. Rahuman, G. Rajakumar, S. Marimuthu, *et al.* Acaricidal, pediculocidal and larvicidal activity of synthesized ZnO nanoparticles using wet chemical route against blood feeding parasites, *Parasitol. Res.*, 2011, **109**, 461–472.
13 A. Alkaladi, A. M. Abdelazim and M. Afifi, Antidiabetic Activity of Zinc Oxide and Silver Nanoparticles on Streptozotocin-Induced Diabetic Rats, *Int. J. Mol. Sci.*, 2014, **15**, 2015–2023.
14 N. A. Samat and R. M. Nor, Sol–gel synthesis of zinc oxide nanoparticles using *Citrus aurantifolia* extracts, *Ceram. Int.*, 2013, **39**, S545–S548.
15 P. Rajiv, S. Rajeshwari and R. Venckatesh, Bio-Fabrication of zinc oxide nanoparticles using leaf extract of *Parthenium hysterophorus* L. and its size-dependent antifungal activity against plant fungal pathogens, *Spectrochim. Acta, Part A*, 2013, **112**, 384–387.

16 S. Gunalan, S. Rajeshwari and R. Venckatesh, Green synthesized ZnO nanoparticles against bacterial and fungal pathogens, *Progress in Natural Science: Materials International*, 2012, **22**(6), 693–700.
17 J. Qu, X. Yuan, X. Wang and P. Shao, Zinc accumulation and synthesis of ZnO nanoparticles using *Physalis alkekengi* L, *Environ. Pollut.*, 2011, **159**(7), 1783–1788.
18 E. Jiménez-Ferrer, J. Alarcón-Alonso, A. Aguilar-Rojas, A. Zamilpa, *et al.* Diuretic effect of compounds from *Hibiscus sabdariffa* by modulation of the aldosterone activity, *Planta Med.*, 2012, **78**(18), 1893–1898.
19 A. Sharaf, The pharmacological characteristics of *Hibiscus sabdariffa* L, *Planta Med.*, 1962, **10**, 48–52.
20 N. Salleh, I. Runnie, D. Roach, S. Mohamed, *et al.* Inhibition of low-density lipoprotein oxidation and upregulation of low-density lipoprotein receptor in HepG2 cells by tropical plant extracts, *J. Agric. Food Chem.*, 2002, **50**, 3693–3697.
21 H. H. Lin, J. H. Chen and C. J. Wang, Chemopreventive properties and molecular mechanisms of the bioactive compounds in *Hibiscus sabdariffa* Linn., *Curr. Med. Chem.*, 2011, **18**(8), 1245–1254.
22 T. O. Ajiboye, N. A. Salawu, M. Y. Yakubu, A. T. Oladiji, *et al.* Antioxidant and drug detoxification potentials of *Hibiscus sabdariffa* anthocyanin extract, *Drug Chem. Toxicol.*, 2011, **34**, 109–115.
23 M. Fullerton, J. Khatiwada, J. U. Johnson and S. Davis, Determination of Antimicrobial Activity of Sorrel (*Hibiscus sabdariffa*) on *Esherichia coli* O157:H7 Isolated from Food, Veterinary, and Clinical Samples, *J. Med. Food*, 2011, **14**(9), 950–956.
24 I. Alshami and A. E. Alharbi, Antimicrobial activity of *Hibiscus sabdariffa* extract against uropathogenic strains isolated from recurrent urinary tract infections, *Asian Pac. J. Trop. Dis.*, 2014, **4**(4), 317–322.
25 D. Saravanan, I. A. Lakshmi, M. Gobinath and B. G. Kumar, Potential Antioxidant, Hypoglycemic and Hypolipidemic Effect of Leaves of *Hibiscus platanifolius* Linn., *Int. J. Pharm. Sci. Drug Res.*, 2011, **3**(3), 236–240.
26 A. O. Ademiluyi and G. Oboh, Aqueous extracts of Roselle (*Hibiscus sabdariffa* Linn.) varieties inhibit α-amylase and α-glucosidase activities *in vitro*, *J. Med. Food*, 2012, **16**(1), 88–93.
27 A. Luximon-Ramma, T. Bahorun, M. A. Soobrattee, O. I. Aruoma, *et al.* Antioxidant activities of phenolic, proanthocyanidin, and flavonoid components in extracts of Cassia fistula, *J. Agric. Food Chem.*, 2002, **50**(18), 5042–5047.
28 S. Ghosh, S. Patil, M. Ahire, R. Kitture, *et al.* Synthesis of silver nanoparticles using *Dioscorea bulbifera* tuber extract and evaluation of its synergistic potential in combination with antimicrobial agents, *Int. J. Nanomed.*, 2012, **7**, 483–496.
29 N. Bala, A. Dey, S. Das, R. Basu and P. Nandy, Effect of Hydroxyapatite nanorod on chickpea (*Cicer arietinum*) plant growth and its possible use as nano-fertilizer, *Iran. J. Plant Physiol.*, 2014, **4**(3), 1061–1069.
30 B. Thayumanavan and S. Sadasivam, Physicochemical basis for the preferential uses of certain rice varieties, *Qual. Plant. – Plant Foods Hum. Nutr.*, 1984, **34**(4), 253–257.
31 A. M. Awwad, N. M. Salem and A. O. Abdeen, Biosynthesis of Silver Nanoparticles using *Olea europaea* Leaves Extract and its Antibacterial Activity, *Nanosci. Nanotechnol.*, 2012, **2**(6), 164–170, DOI: 10.5923/j.nn.20120206.03.
32 Z. W. Atwan and F. Saiwan, The antibacterial activity of cold aqueous and pigment of hibiscus *Rosa sinensis* extracts against gram positive and negative bacteria, *Bas. J. Vet. Res.*, 2010, **10**(2), 109–118.
33 S. Mukherjee, V. Sushma, S. Patra, A. K. Barui, *et al.* Green chemistry approach for the synthesis and stabilization of biocompatible gold nanoparticles and their potential applications in cancer therapy, *Nanotechnology*, 2012, **23**(45), 455103.
34 R. K. Das, N. Gogoi, P. J. Babu and P. Sharma, The Synthesis of Gold Nanoparticles Using *Amaranthus spinosus* Leaf Extract and Study of Their Optical Properties, *Adv. Mater. Phys. Chem.*, 2012, **2**, 275–281.
35 Z. R. Khan, M. S. Khan, M. Zulfequar and M. S. Khan, Optical and Structural Properties of ZnO Thin Films Fabricated by Sol–Gel Method, *Mater. Sci. Appl.*, 2011, **2**, 340–345.
36 J. Mariajancyrani, G. Chandramohan and R. Ravikumar, Isolation and identification of phytoconstituents from *Delonixregia* leaves, *Int. J. Pharm. Pharm. Sci.*, 2013, **5**(S4), 671–674.
37 A. J. D. Britto, D. H. S. Gracelin and P. B. J. R. Kumar, Qualitative and quantitative analysis of phytochemicals in *Marsilea minuta* Linn., *Int. J. Pharma Bio Sci.*, 2013, **4**(1), 800–805.
38 P. J. P. Espitia, N. F. F. Soares, J. S. R. Coimbra, N. J. Andrade, R. S. Cruz and E. A. A. Medeiros, Zinc Oxide Nanoparticles: Synthesis, Antimicrobial Activity and Food Packaging Applications, *Food Bioprocess Technol.*, 2012, **5**, 1447–1464.
39 N. Jones, B. Ray, K. T. Ranjit and A. C. Manna, Antibacterial activity of ZnO nanoparticle suspensions on a broad spectrum of microorganisms, *FEMS Microbiol. Lett.*, 2008, **279**, 71–76.
40 M. M. Cowan, Plant products as antimicrobial agents, *Clin. Microbiol. Rev.*, 1999, **12**, 564–582.
41 S. E. Walsh, J. Y. Maillard, A. D. Russel, C. E. Catrenich, *et al.* Activity and mechanism of action of selected biocidal agents on gram -positive and -negative bacteria, *J. Appl. Microbiol.*, 2003, **94**, 240–247.
42 A. E. Butler, J. Janson, S. Bonner-Weir, *et al.* Beta-cell deficit and increased beta-cell apoptosis in humans with type 2 diabetes, *Diabetes*, 2003, **52**, 102–110.
43 J. F. Navarro-González and C. Mora-Fernández, The role of inflammatory cytokines in diabetic nephropathy, *J. Am. Soc. Nephrol.*, 2008, **19**, 433–442.
44 X. Gao, A. BelmadaniS, A. Picchi, X. Xu, *et al.* Tumor necrosis factor-alpha induces endothelial dysfunction in Lepr(db) mice, *Circulation*, 2007, **115**, 245–254.
45 A. Tahrani, K. Milan, K. Amy and H. Anthony, Glycaemic control in type 2 diabetes: targets and new therapies, *Pharmacol. Ther.*, 2010, **12**, 328–361.
46 L. Orci, R. H. Unger and M. Ravazzola, Reduced β-cell glucose transporter in new onset diabetic BB rats, *J. Clin. Invest.*, 1990, **86**, 1615–1622.

47 W. J. Schnedl, S. Ferber, J. H. Johnson and C. B. Newgard, STZ transport and cytotoxicity: specific enhancement in *GLUT 2*-expressing cells, *Diabetes*, 1994, **43**, 1326–1333.
48 K. D. Kröncke, K. Fehsel, A. Sommer, M. L. Rodriguez and V. Kolb-Bachofen, Nitric oxide generation during cellular metabolization of the diabetogenic *N*-methyl-*N*-nitroso-urea streptozotocin contributes to islet cell DNA damage, *Biol. Chem. Hoppe-Seyler*, 1995, **376**, 179–185.
49 M. Elsner, B. Guldbakke, M. Tiedge, R. Munday and S. Lenzen, Relative importance of transport and alkylation for pancreatic beta-cell toxicity of streptozotocin, *Diabetologia*, 2000, **43**, 1528–1533.
50 T. Szkudelski, The Mechanism of Alloxan and Streptozotocin Action in B Cells of the Rat Pancreas, *Physiol. Res.*, 2001, **50**, 536–546.
51 G. Dodson and D. Steiner, The role of assembly in insulin's biosynthesis, *Curr. Opin. Struct. Biol.*, 1988, **8**, 189–194.
52 E. R. Arquilla, S. Packer, W. Tarmas and S. Miyamoto, The effect of zinc on insulin metabolism, *Endocrinology*, 1978, **103**, 1440–1449.
53 A. B. Chausmer, Zinc, insulin and diabetes, *J. Am. Coll. Nutr.*, 1998, **17**, 109–115.
54 V. K. Garg, R. Gupta and R. K. Goyal, Hypozincemia in diabetes mellitus, *J. Assoc. Phys. India*, 1994, **42**, 720–721.
55 C. H. Peng, C. C. Chyau, K. C. Chan, *et al. Hibiscus subdariffa* polyphenolic extract inhibits hyperglycemia, hyperlipidemia, and glycation-oxidative stress while improving insulin resistance, *J. Agric. Food Chem.*, 2011, **59**(18), 9901–9909.
56 N. K. Choudhary, A. K. Jha, S. Sharma and S. Goyal, Anti-diabetic potential of chloroform extract of flowers of *Calotropis gigantea*: an *in vitro* and *in vivo* study, *Int. J. Green Pharm.*, 2011, **5**, 296–301.
57 K. B. Pandey and S. I. Rizvi, Plant polyphenols as dietary antioxidants in human health and disease, *Oxid. Med. Cell. Longevity*, 2009, **2**(5), 270–278.